Observations of urban heat island advection from a high-density monitoring network

Bassett, Richard; Cai, Xiaoming; Chapman, Lee; Heaviside, Clare; Thornes, John; Muller, Catherine; Young, Duick; Warren, Elliott

DOI:
10.1002/qj.2836

Document Version
Publisher's PDF, also known as Version of record

Citation for published version (Harvard):
Bassett, R, Cai, X, Chapman, L, Heaviside, C, Thornes, J, Muller, C, Young, D & Warren, E 2016, 'Observations of urban heat island advection from a high-density monitoring network', *Quarterly Journal of the Royal Meteorological Society*, vol. 142, no. 699, pp. 2434–2441. https://doi.org/10.1002/qj.2836

RMetS
Royal Meteorological Society

Observations of urban heat island advection from a high-density monitoring network

Richard Bassett,[a] Xiaoming Cai,[a]* Lee Chapman,[a] Clare Heaviside,[a,b] John E. Thornes,[a,b] Catherine L. Muller,[a] Duick T. Young[c] and Elliott L. Warren[a]

[a]*School of Geography, Earth and Environmental Sciences, University of Birmingham, UK*
[b]*Environmental Change Department, Centre for Radiation, Chemical and Environmental Hazards, Public Health England, Didcot, UK*
[c]*Department of Meteorology, University of Reading, UK*

*Correspondence to: X.-M. Cai, School of Geography, Earth and Environmental Sciences, University of Birmingham, B15 2TT, UK. E-mail: x.cai@bham.ac.uk

With 69% of the world's population predicted to live in cities by 2050, modification to local climates, in particular Urban Heat Islands (UHIs), have become a well studied phenomenon. However, few studies have considered how horizontal winds modify the spatial pattern in a process named Urban Heat Advection (UHA) and this is most likely due to a lack of highly spatially resolved observational data. For the first time, this study separates the two-dimensional advection-induced UHI component, including its pattern and magnitude, from the locally heated UHI component using a unique dataset of urban canopy temperatures from 29 weather stations (3 km resolution) recorded over 20 months in Birmingham, United Kingdom. The results show that the mean contribution of UHA to the warming of areas downwind of the city can be up to 1.2 °C. Using the inverse Normalized Difference Vegetation Index as a proxy for urban fraction, an upwind distance at which the urban fraction has the strongest correlation with UHA was demonstrated to be between 4 and 12 km. Overall, these findings suggest that urban planning and risk management needs to additionally consider UHA. However, more fundamentally, it highlights the importance of careful interpretation of long- term meteorological records taken near cities when they are used to assess global warming.

Key Words: advection; heat; sensors; temperature; urban; urban heat advection; urban heat island; wind

Received 6 November 2015; Revised 29 April 2016; Accepted 5 May 2016; Published online in Wiley Online Library

1. Introduction

It is well documented that urban conurbations are warmer than their rural surroundings (Arnfield, 2003; Stewart, 2011). The resulting phenomenon, known as the urban heat island (UHI), develops through the absorption of energy within the built environment during the day, and subsequent release at night. The structure and intensity of the UHI are controlled by the city form and are a direct result of anthropogenic modifications to the surface energy balance (Oke, 1973, 1982). These changes include: reduced sky view factor (fraction of visible sky from the ground) restricting long-wave radiation loss at night; different thermal and reflective properties from construction materials; reduced evapotranspiration due to less vegetation; lower wind speeds (increased surface roughness); and anthropogenic heat from buildings, people and vehicles. Cities typically exhibit spatial variations in UHI intensity that can be broadly classified into Local Climate Zones (LCZ), which are effectively determined by land use (Stewart and Oke, 2012). Alternatively, land cover products, for example vegetation indices derived from remote sensing, can used to assess UHI intensity (Chen *et al.,* 2006). The largest UHI intensities are generally found in the central business districts under clear skies and calm winds, whereas more turbulent conditions increase mixing and weaken UHIs.

The significance of the UHI effect becomes increasingly apparent by studying interactions with the health and well-being of the local population. For example, in England and Wales, 81.5% of the population are urbanised (ONS, 2013) and with cities unable to cool down as efficiently as their surroundings, there is a growing heat-health and infrastructure risk (Grimmond *et al.*, 2010; Thornes, 2015). UHI impacts are further compounded during heatwave events. It is estimated that the 2003 summer heatwave led to as many as 70 000 excess deaths throughout Europe (Robine *et al.*, 2008), 2000 of which were in England (Johnson *et al.*, 2005). Climate projections (e.g. UKCP09: http://ukclimateprojections.metoffice.gov.uk/) indicate that heatwaves will become an increasingly regular feature of the UK climate before the end of the century, underlining the need for increased mitigatory action to protect vulnerable populations and critical infrastructure (Chapman *et al.*, 2013). Until recently, a lack of external influence has left urban planning to habitually follow historical architecture, based on local climate and culture

(Grimmond *et al.*, 2010). However, with a changing climate, historical designs may no longer be adequate to cope with an increase in excess heat, particularly during heatwaves. In response, cities are progressively developing adaptation strategies to cope with the effects of excess heat on health and infrastructure. However, to efficiently target strategies and resources (e.g. green infrastructure), a complete picture of how UHIs develop temporally and spatially is needed.

Lowry (1977) conceptually proposed that the 'environ' or area of urban influence on surrounding rural temperatures is not stationary and is in fact determined by weather type. Despite the abundance of studies into the UHI effect (Arnfield, 2003; Stewart, 2011) and the impact of urbanisation on climate (Kalnay and Cai, 2003; Zhou *et al.*, 2004), few studies have considered (or assumed it not to be significant) how horizontal winds modify the urban environ through the advection-induced UHI component – a process named Urban Heat Advection (UHA).

Oke (1976) highlighted the distinction between processes in the urban canopy layer (UCL) and urban boundary layer (UBL). The UCL extends from the surface to the mean building roof level, and within the UCL canopy-scale processes will influence local UHI values significantly. Whilst winds could effectively move or advect heat (and moisture) horizontally within the UCL (from micro- to neighbourhood-scale), other UHA processes may occur in the UBL (from neighbourhood- to city-scale). Heat released from urban facets (building surfaces, roads etc.) is transferred (through the turbulent roughness sub-layer) from the UCL into the UBL aloft. The buoyant, rising air (forming a thermal dome) over the urban environment at a city scale creates a pressure field that draws in rural air (Barlow, 2014). This can lead to three-dimensional circulations in the form of surface convergence over the city and divergence aloft (Bornstein and Johnson, 1977; Hildebrand and Ackerman, 1984; Hidalgo *et al.*, 2010). If a horizontal wind is present, and prevails over local circulations, a thermal plume from the UCL becomes vertically mixed and subsequently advected downwind (Clarke, 1969; Oke, 1982). Observations during the METROMEX field campaign indicated that advection modulates downwind sensible heat fluxes (Ching *et al.*, 1983; Godowitch *et al.*, 1987) and urban plumes were shown to typically extend 10–15 km downwind (Dirks, 1974; Wong and Dirks, 1978). Between the neighbourhood and city scales, the heterogeneous nature of urban environments acts to create a series of overlapping local internal boundary layers (Garratt, 1990; Barlow, 2014). Over a warmer UCL, heat will be transferred upward from the UCL to the UBL, whereas over a cooler UCL, downward heat flux is likely to occur. However, little is known about the mechanisms of the two processes, particularly the latter, i.e. how much heat from these urban plumes is mixed downwards into the UCL to warm the air underneath. Furthermore the vertical scale of the UBL varies diurnally. A well-developed UBL during the day (1–2 km) will allow plumes to spread high into the UBL. However at night the UBL becomes typically limited to a few hundred metres at night, capped by stable air above. On this basis, heat will not be dispersed vertically as far from the UCL at night as is possible during the day.

Prior investigations into UHA have been attempted using temperature data collected from two related methodologies: (i) mobile sensors based on a traverse (Brandsma and Wolters, 2012; Unger *et al.*, 2010) and (ii) fixed sensors at weather stations in the region (Chandler, 1965; Brandsma *et al.*, 2003; Haeger-Eugensson and Holmer, 1999; Gedzelman, 2003; Takane *et al.*, 2013). In addition to presenting the spatial patterns of UHI, not UHA, a limitation of these methodologies is a general inability to demonstrate the high-resolution two-dimensional structure of UHA with any statistical confidence due to either temporal or spatial limitations of the chosen approach. Typically, the method of using mobile sensors along transects suffers from short duration of measurement, whereas the method of using fixed sensors at stations is constrained by the small number of stations. For example the METROMEX campaign demonstrated wind modifications to the UHI (Ackerman *et al.*, 1978); however, the UHA signals were weak due to the coarse spatial resolution (horizontal resolution of about 13 km) and because not all observations were within the UCL. Given these constraints, recent attempts to quantify UHA have focussed on modelling approaches to enable the simulation of spatial dimensions that observations have, to date, been unable to capture (e.g. Zhang *et al.*, 2009; Bohnenstengel *et al.*, 2011; Chemel and Sokhi, 2012; Heaviside *et al.*, 2015). Remote-sensing techniques have also been increasingly used to capture the spatial nature of surface UHI (Tomlinson *et al.*, 2012, 2013). However, satellite-derived surface UHI are not always directly comparable with UCL UHI (air temperature). It is hypothesised that advection is a key cause for this difference because the surface UHI remains static (i.e. linked to underlying land use), whereas the UCL UHI is much more dynamic due to wind effects (Azevedo *et al.*, 2016).

Fundamentally, a lack of high-quality dense urban networks has restricted the study of UHA features (Muller *et al.*, 2013), largely due to the difficulty and cost of siting and maintaining urban networks (Chapman *et al.*, 2014). This paucity of data has resulted in previous observational studies relying on a transect approach and modelling approaches limited by a lack of evaluation data. To overcome this challenge this article presents the two-dimensional pattern and magnitude of the advection-induced UHI component, UHA, under various wind speeds and directions at the city scale using a new high-resolution urban meteorological observational dataset. In doing so, a quantification of UHA is achieved which can be used strategically to mitigate heat impacts of upwind local climate on downwind populations. It also enables a critical view of whether rural reference stations commonly used in UHI studies are truly representative of the background climate due to possible contamination by UHA, which has potential implications on the accuracy of temperature records used for analyses of global warming.

2. Methods and background

2.1. Study area and data

A new network of automatic weather stations – the Birmingham Urban Climate Laboratory (BUCL) has been installed across Birmingham (52.5°N, 1.9°W, Figure 1), the United Kingdom's second largest city with 1.1 million inhabitants, specifically to

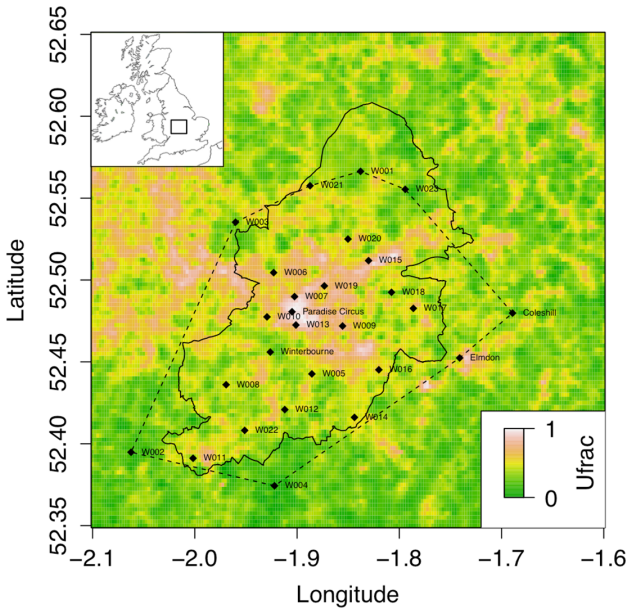

Figure 1. Study area and location of BUCL stations, and urban fraction (Ufrac), ranging from 0 (rural) to 1 (urban). Birmingham's administrative region is outlined with a solid border. The dashed border indicates the outer boundary of observations.

Table 1. Station metadata. Local Climate Zones (LCZ) are assigned using the classification by Stewart and Oke (2012). Urban fraction is calculated as the mean pattern within a 1 km radius of each station.

Station	Network	Latitude	Longitude	Altitude (m)	Urban fraction (1 km radius)	LCZ
W001	BUCL	52.57	−1.84	119	0.36	Scattered trees
W002	BUCL	52.39	−2.06	187	0.23	Scattered trees
W003	BUCL	52.54	−1.96	104	0.38	Scattered trees
W004	BUCL	52.37	−1.92	202	0.16	Scattered trees
W005	BUCL	52.44	−1.86	158	0.49	Open low rise
W006	BUCL	52.5	−1.92	132	0.6	Open low rise
W007	BUCL	52.49	−1.90	134	0.83	Compact mid rise
W008	BUCL	52.44	−1.97	168	0.45	Open low rise
W009	BUCL	52.47	−1.86	123	0.7	Compact mid rise
W010	BUCL	52.48	−1.93	157	0.61	Open low rise
W011	BUCL	52.39	−2.00	190	0.51	Open low rise
W012	BUCL	52.42	−1.91	134	0.5	Open low rise
W013	BUCL	52.47	−1.90	125	0.82	Compact mid rise
W014	BUCL	52.42	−1.84	141	0.5	Open low rise
W015	BUCL	52.51	−1.83	98	0.68	Heavy industry
W016	BUCL	52.45	−1.82	130	0.53	Open low rise
W017	BUCL	52.48	−1.79	101	0.52	Open low rise
W018	BUCL	52.49	−1.81	100	0.48	Open low rise
W019	BUCL	52.50	−1.87	110	0.74	Open mid rise
W020	BUCL	52.53	−1.85	140	0.55	Open low rise
W021	BUCL	52.56	−1.89	173	0.51	Open low rise
W022	BUCL	52.41	−1.95	150	0.47	Open low rise
W023	BUCL	52.56	−1.79	122	0.32	Open low rise
W026	BUCL	52.46	−1.93	150	0.41	Open low rise
W027	BUCL	52.44	−1.89	158	0.49	Open low rise
Coleshill	Met Office	52.48	−1.69	96	0.39	Scattered trees
Elmdon	Met Office	52.45	−1.74	96	0.61	Open mid rise
Paradise Circus	Met Office	52.48	−1.90	139	0.9	Compact high rise
Winterbourne	Met Office	52.46	−1.93	140	0.4	Open low rise

study city-scale weather processes using stations within the UCL. The BUCL network consists of two arrays of weather monitoring equipment and this study utilises data from the coarse array of 25 automatic weather stations (Vaisala WXT520, accurate to $\pm 0.3\,^{\circ}$C at 20 °C: Vaisala, 2012) that records minute averages of air temperature, relative humidity, atmospheric pressure, wind speed and direction, and precipitation at 3 m above ground. Guidelines on siting instruments in urban areas (Oke, 2006) were adhered to where possible when the network was installed with most stations sited within school grounds. A full description of the network can be found in Chapman *et al.* (2014) and is further documented via a new urban metadata protocol devised during the deployment (Muller *et al.*, 2013). Observations are also taken from four UK Met Office weather stations accessed through the British Atmospheric Data Centre: Paradise Circus, Winterbourne, Elmdon and Coleshill. In total 29 stations provide coverage across Birmingham at approximately 3 km resolution (Table 1; Figure 1). To represent an unobstructed synoptic flow, wind data are taken from Coleshill, at a height of 10 m, due to its location outside the city. Data for this study were obtained from 1 January 2013 to 1 September 2014. The network and data undergo a rigorous process of quality assurance and control. Full descriptors of the data quality assurance procedures are documented in Warren *et al.* (2016) complete with repository links directly to the data and associated metadata.

In addition to the meteorological data, the normalized difference vegetation index (NDVI), a readily available MODerate-resolution Imaging Spectroradiometer (MODIS) product already used in UHI studies (e.g. Chen *et al.*, 2006), is used to indicate urban fraction across Birmingham. The mean NDVI is calculated from averaging a 250 m resolution January and July 2014 (16-day composite) image to account for seasonality in leaf coverage. From herein the NDVI data, normalised to between 0 (rural) and 1 (urban), is referred to as urban fraction (Ufrac).

2.2. Urban heat island

UHI intensity is traditionally calculated by taking the temperature difference between an urban and a rural reference station (Arnfield, 2003; Stewart, 2011). However, this approach is challenged by the fact that rural reference stations near cities may be influenced by UHA if they are located within the urban environ as demonstrated conceptually by Lowry (1977) and directly in the region of study through modelling (Heaviside *et al.*, 2015). To minimise this influence by UHA, a new concept of 'inverse UHI' is introduced, which adopts temperatures at a central urban station (T_u) as reference. The Met Office station at Paradise Circus is chosen to represent the central urban station (T_u) due to its location within the centre of Birmingham and is the station where the highest temperatures have been identified in previous studies (Tomlinson *et al.*, 2012, 2013; Heaviside *et al.*, 2015). The hourly temperature difference (ΔT_{i-u}) between each station in the network (T_i, where i denotes the ith station) and the central urban station (T_u) is calculated for the data period (Eq. (1)):

$$\Delta T_{i-u} = T_i - T_u. \quad (1)$$

The value of this temperature difference (ΔT_{i-u}) will be mostly negative as the central urban station (T_u) is likely to be higher than other stations in the network (T_i). Temperature data are split equally into three wind-speed groups, WG1 ($<2\,\mathrm{m\,s^{-1}}$), WG2 ($2-3\,\mathrm{m\,s^{-1}}$) and WG3 ($>3\,\mathrm{m\,s^{-1}}$). Only night-time observations (based on daily sunset and sunrise times) with low cloud cover ($<4/8$ oktas) are included, to focus on conditions most favourable for strong UHI development. Classifying by wind speed, cloud cover and night-time, groups the data into conditions of similar stability (neutral and stable) as per Pasquill–Gifford stability classes (Pasquill and Smith, 1983; Tomlinson *et al.*, 2012). The mean temperature difference within each wind speed group is taken ($\overline{\Delta T_{i-u}}$). The assumption is made that the mean difference between the ith station and central urban station (T_u) remains constant within these stability classifications, thereby compensating for some stations not being temporally homogeneous. In order to interpret the magnitude of the mean temperature difference ($\overline{\Delta T_{i-u}}$) as the positive UHI intensity, the minimum temperature difference in each wind speed group is

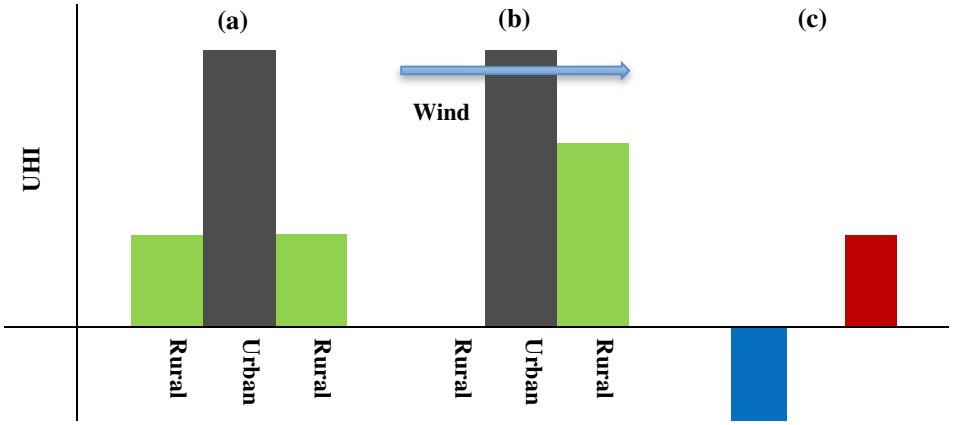

Figure 2. Hypothetical advection calculation (adapted from Heaviside *et al.*, 2015). Illustration (a) signifies a typical time-mean UHI, assuming that the advection-induced warming is symmetric with respect to two wind directions under the same wind speed and stability group. Therefore, both rural columns will be warmed and the magnitude of the positive bar over the right rural area in (a) is effectively a half of the magnitude of the UHI due to advection in (b). Illustration (b) considers a single wind direction, left to right, and this hypothetically means no heat is transferred upwind from the urban to left rural column (n.b. the rural background temperature, created by local land use, does not decrease). Illustration (c) is derived by subtracting (a) from (b), i.e. removing the locally heated UHI component (the middle positive bar) and separating the advection-induced component. The negative value in (c) is linked to UHA from the opposing wind direction. The difference between positive and negative bars in (c) is interpreted as the UHA signal.

subtracted from each station. The resulting positive UHI intensity is denoted by $\overline{\Delta T^{+}}$.

2.3. Urban heat advection

As discussed in section 1, the environ (or area) of influence exerted by a city on its surroundings varies dimensionally. Lowry's (1977) working model (Eq. (2)) states the temperature (T, or other element) at a given station i, time t, and weather type x is a sum of the background temperature (B), and deviation caused by landscape (L, e.g. relief) and urban effects (U). If landscape effects are comparable at two given stations (rural and urban), any temperature difference can be attributed to urban effects. However, in practice, a given rural station may be influenced by the urban environ under particular weather type (or wind direction), and therefore the temperature difference is not an accurate reflection on UHI intensity. Lowry's (1977) model is therefore unable to distinguish between urban effects, i.e. heat created locally or advected from upwind. As such, Lowry's (1977) concept should be enhanced through separating urban effects (U) at a given location into contributing terms: local UHI, and additional UHA (Eq. (3)). Separating these terms however is complicated by the fact that observed data combines information on both processes.

$$\mathrm{T}_{i,t,x} = \mathrm{B}_{i,t,x} + \mathrm{L}_{i,t,x} + \mathrm{U}_{i,t,x}, \tag{2}$$

$$\mathrm{T}_{i,t,x} = \mathrm{B}_{i,t,x} + \mathrm{L}_{i,t,x} + (\mathrm{UHI}_{i,t,x} + \mathrm{UHA}_{i,t,x}). \tag{3}$$

In order to separate UHA from UHI, a methodology used in Weather Research and Forecasting (WRF) modelling of the August 2003 heatwave (Heaviside *et al.*, 2015) is adapted for the BUCL observation network. Here, the time-mean temperature field is subtracted from the averaged modelled field for each of four specified wind directions at 90° intervals (θ: northeast (NE), southeast (SE), southwest (SW) and northwest (NW)). A hypothetical example is presented in Figure 2, whereby this methodology decomposes the UHI into the time-mean component (predominantly dependent of local land surface) and a horizontally advected component. To calculate the mean UHA at the ith station in the BUCL network, ($\overline{T^{(\theta)}_{UHA\ (i)}}$), the temperature field ($\overline{\Delta T_{i-\mathrm{u}}}$) across all wind directions is subtracted from the mean temperature difference for a given wind direction sector (θ), ($\overline{\Delta T^{(\theta)}_{i-\mathrm{u}}}$), shown in Eq. (2). An example calculation is presented in Figure 3(a). To account for any directional biases within the data, the temperature field across all wind directions ($\overline{\Delta T_{i-\mathrm{u}}}$) used in Eq. (4) is calculated by taking the mean of the mean temperature difference of each wind sector, ($\overline{\Delta T^{(\theta)}_{i-\mathrm{u}}}$), Eq. (5).

$$\overline{T^{(\theta)}_{UHA\ (i)}} = \overline{\Delta T^{(\theta)}_{i-\mathrm{u}}} - \overline{\Delta T_{i-\mathrm{u}}}, \tag{4}$$

$$\overline{\Delta T_{i-\mathrm{u}}} = \frac{(\Delta T^{(\mathrm{NE})}_{i-\mathrm{u}} + \Delta T^{(\mathrm{SE})}_{i-\mathrm{u}} + \Delta T^{(\mathrm{NW})}_{i-\mathrm{u}} + \Delta T^{(\mathrm{SW})}_{i-\mathrm{u}})}{4}. \tag{5}$$

By calculating the mean UHA for a given wind sector, $\overline{T^{(\theta)}_{UHA\ (i)}}$, the positive value is interpreted as half the advection-induced UHI component and the negative value is half the advection-induced UHI component from the opposing wind direction (Figure 2(c)). As such, UHA can be interpreted as the difference between these two values (n.b. upwind and downwind values will swap with opposing wind directions), and free from background, landscape and UHI effects. Whilst this approach distinguishes between each component in Lowry's (1977) model, it is unable to determine the process and scale at which UHA occurs (i.e. horizontally through the UCL or downwards mixing from the thermal plume), as vertical observations are not available.

2.4. Urban heat advection distance

To investigate the spatial scale at which UHA occurs, concentric annuli (*ann*) at 3 km intervals extending 0–3, 4–6, 7–9, 10–12 and 13–15 km from each station (i) are overlaid onto the Ufrac data (Figure 3). Within each of the five annuli, the mean urban fraction is calculated, referred to as $Ufrac^{(ann)}_{(i,\,d)}$, where d is the index of the annuli (i.e. $d=1$: 0–3 km; $d=2$: 4–6 km; ... $d=5$: 13–15 km). Each annulus is further split by the four wind direction sectors (θ) to create four arcs, and for each θ, the mean urban fraction is calculated, referred to as $Ufrac^{(\theta)}_{(i,d)}$. A similar methodology used to calculate the mean UHA for a given wind sector ($\overline{T^{(\theta)}_{UHA\ (i)}}$) is then applied to the Ufrac data. Namely, at a given station i and distance d, the Ufrac annuli $Ufrac^{(ann)}_{(i,d)}$ is subtracted from the Ufrac arc $Ufrac^{(\theta)}_{(i,d)}$ (Eq. (6)):

$$\overline{\Delta Ufrac^{(\theta)}_{(i,d)}} = \overline{Ufrac^{(\theta)}_{(i,d)}} - \overline{Ufrac^{(ann)}_{(i,d)}}. \tag{6}$$

This quantity, $\overline{\Delta Ufrac^{(\theta)}_{(i,d)}}$, reflects the directional inhomogeneity, or variability of urban land use, of the dth annulus, i.e. whether the urban fraction value in a given direction is higher or

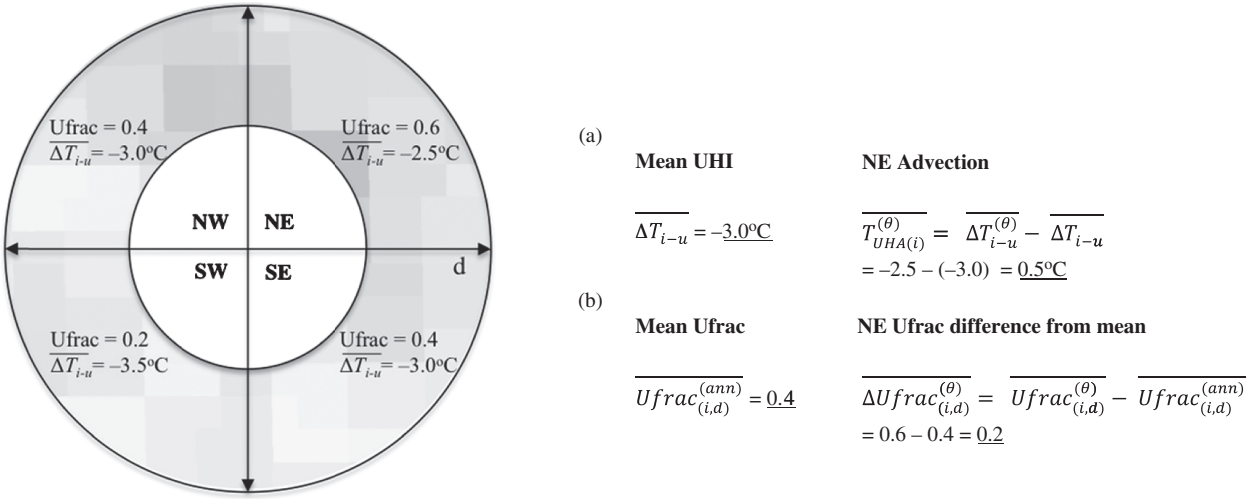

Figure 3. Hypothetical explanation of how (a) UHA ($\overline{T^{(\theta)}_{UHA(i)}}$) and (b) Ufrac difference from the mean ($\overline{\Delta Ufrac^{(\theta)}_{(i,d)}}$) are calculated under a NE wind for a given station (i) located in the centre of the crosshairs. The temperature difference ($\overline{\Delta T^{(\theta)}_{i-u}}$) has a smaller magnitude from the NE (more urbanised sector), i.e. the actual temperature is closer to the urban reference than SW (less urbanised sector).

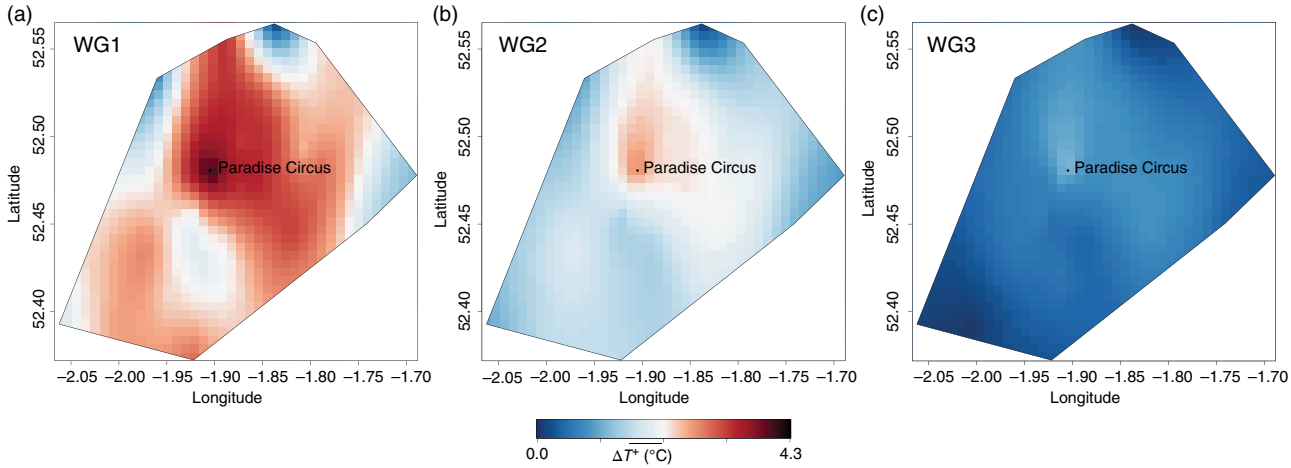

Figure 4. Spatial interpolation (kriging) of the nocturnal positive UHI intensity ($\overline{\Delta T^{+}}$) under low cloud cover in three wind-speed groups: (a) WG1 (<2 m s^{-1}), (b) WG2 (2–3 m s^{-1}) and (c) WG3 (>3 m s^{-1}). The analysis is limited to the outer boundary of observations.

lower than the mean of all directions. A hypothetical calculation is shown in Figure 3(b). In order to generate statistically meaningful correlations between UHA and directional variability of upwind urban fractions, stations in the network with little Ufrac variation between arcs (<0.1 range) are excluded from the analysis. Whilst the station data are grouped for similar stability, there are still differences in the mean UHI and UHA for each wind direction explained by meteorological differences within wind groups that cannot be accounted for. For example the data are categorised into less than 4/8 oktas; however ,within this group winds from the SE may have a higher percentage of completely clear skies. Finally, to account for directional differences, normalised UHI and UHA values for each wind direction are taken.

3. Results and discussion

3.1. Urban heat island

Ordinary kriging (R 'kriging' package version 1.1) is used to interpolate the positive UHI intensity ($\overline{\Delta T^{+}}$) for each wind speed group (Figure 4). Interpolation predicts temperatures at unmeasured locations using weighted averages from surrounding stations. Kriging-based approaches to spatial interpolation have been used in several UHI studies (e.g. Szymanowski and Kryza, 2009; Knight *et al.*, 2010; Unger *et al.*, 2010; Azevedo *et al.*, 2016). As per Knight *et al.* (2010) the analysis is confined to the outer boundary of observations and only used for visualisation. A large mean night-time UHI intensity under low cloud cover up to 4.3 °C is observed across the region in WG1. Cool spots are found to the north of the city in Sutton Park and directly to the south in notably green urban areas within the city. Both areas are approximately 2 °C cooler and are marked by 'temperature cliffs': a sharp change in temperature over short distances. A decrease in the maximum UHI intensity is found when wind speed increases (WG2: 3.0 and WG3: 1.3 °C) and spatially the heat becomes more confined to the city centre. The observed UHI spatial pattern is found to be similar to satellite and modelling research in Birmingham (Tomlinson *et al.*, 2012, 2013; Heaviside *et al.*, 2015). However, UHI intensities vary between these methodologies due to inherent differences between surface and UCL temperatures.

3.2. Urban heat advection

The resulting mean UHA ($\overline{T^{(\theta)}_{UHA\ (i)}}$) is shown spatially for each wind speed group and sector in Figure 5. The results show that a significant upwind, downwind temperature difference of up to 1.2 °C exists across Birmingham (WG2). The NE and SW cases show a clear downwind warming, present in each wind group, with a transition from a positive to negative warming located over the city centre. The NW case has warming and SE cooling present over the whole domain, in all wind groups. Whilst warming is still most pronounced downwind in the NW case, the cross-domain warming could be accounted for by urbanisation northwest of Birmingham (see Ufrac in Figure 1). Additionally as the analysis is

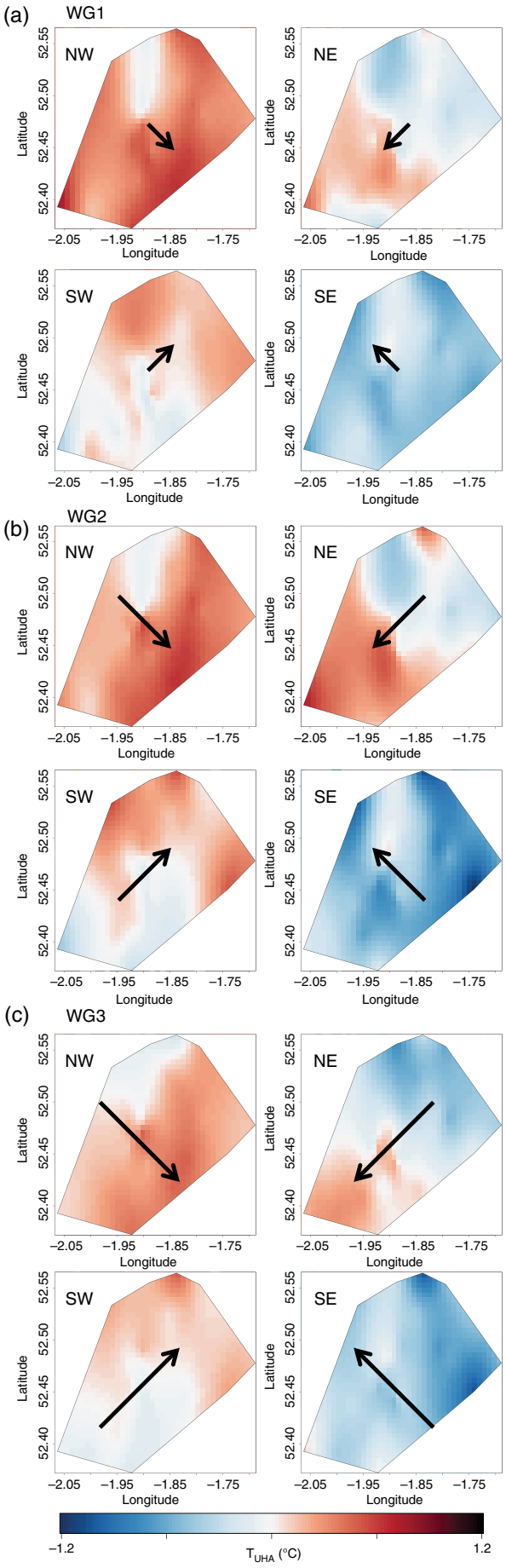

Figure 5. Spatial interpolation (kriging) of UHA ($\overline{T^{(\theta)}_{UHA\ (i)}}$) in three wind speed groups: (a) WG1 (<2 m s^{-1}), (b) WG2 (2–3 m s^{-1}) and (c) WG3 (>3 m s^{-1}). Within each wind speed group, each box represents a wind direction sector (θ: NW, NE, SE, SW).

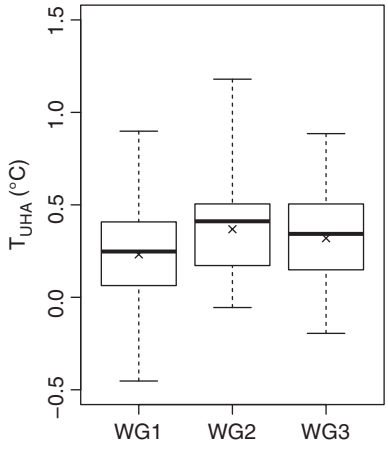

Figure 6. UHA box-and-whisker plot ($\overline{T^{(\theta)}_{UHA\ (i)}}$) using SW and NE wind sectors, in three wind speed groups: WG1 (<2 m s^{-1}), WG2 (2–3 m s^{-1}) and WG3 (>3 m s^{-1}). The × marker signifies the mean.

confined around the city, there are limitations with kriging or any spatial interpolation technique at the edge of a domain. Spatially the results have demonstrated the urban influence, through UHA, to extend outside the city limits. In effect the observed UHA patterns match the hypothetical calculation (Figure 2) and substantiate Lowry's (1977) dynamic urban environ zone.

In order to quantify the mean UHA across all stations, the data are split into two groups of stations that are considered to be upwind or downwind of the city centre. The SW and NE wind sectors, as indicated in Figure 1, are used for this analysis due to the increased number of stations in this direction across the city. The calculated mean UHA ($\overline{T^{(\theta)}_{UHA\ (i)}}$) at each station in the SW and NE groups are combined (i.e. both groups show positive UHA downwind) for each wind speed group (Figure 6). For WG1 a mean UHA across all stations of 0.2 °C is observed. As wind speeds increase (WG2) the mean UHA rises to 0.4 °C. A further increase in wind speed (WG3) reduces mean UHA to 0.3 °C. It is also found that for WG2, UHA reaches 0.5 °C or higher at 25% of stations, up to a maximum of 1.2 °C. A maximum UHA occurring in WG2 could be explained by a reduced capability to advect heat with lower wind speeds, and less heat to advect from a smaller UHI at high wind speeds. This finding is similar to Brandsma *et al.* (2003) who found peak UHA to occur at medium wind speeds between 2.2 and 3.9 m s^{-1}.

The results show that UHA is a significant phenomenon present in the UCL and is not limited to a thermal plume in the UBL (Clarke, 1969; Dirks, 1974; Wong and Dirks, 1978; Oke, 1982). As such this analysis shows that the temperature of a given location is significantly affected by adjacent urban fraction. Additionally, because the UHA components presented in Figures 5 and 6 are temporally averaged over 20 months, it is suggested that UHA could be higher under certain meteorological conditions, for example a heatwave (Heaviside *et al.*, 2015). To place this additional downwind warming in context, a degree temperature difference has the potential to increase mortality by 2% for every degree rise over 17.7 °C in the West Midlands (Hajat *et al.*, 2014; Heaviside *et al.*, 2016).

However whilst UHA is successfully separated from the UHI signal and quantified for Birmingham, these observations are unable to differentiate UHA processes. Further work is needed to explore whether winds move heat horizontally through the UCL, or if urban heat is mixed into the UBL, and then a proportion brought back to the UCL downwind.

3.3. *Urban heat advection distance*

In order to show the relationship between urban fraction the two urban effects UHI and UHA, Pearson's correlation coefficient is firstly conducted across all stations between the Ufrac annuli

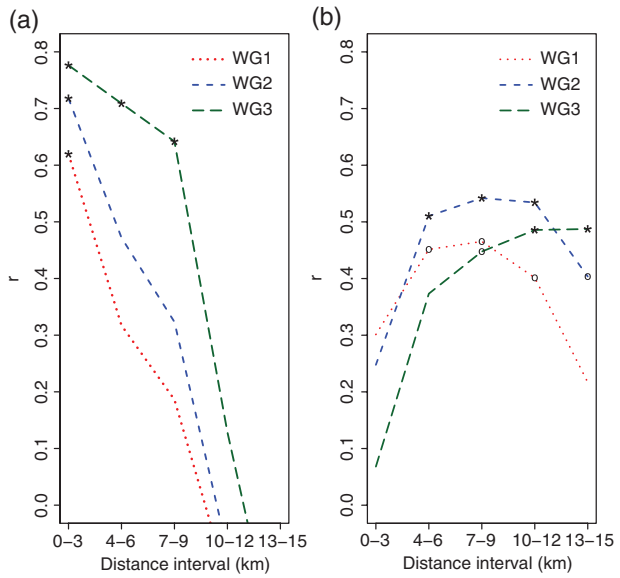

Figure 7. Pearson's correlation coefficient (r) between (a) UHI ($\overline{\Delta T_{i-\mathrm{u}}}$) and Ufrac annuli ($\overline{Ufrac^{(ann)}_{(i,d)}}$), (b) UHA ($\overline{T^{(\theta)}_{UHA\ (i)}}$) and Ufrac arcs ($\overline{\Delta Ufrac^{(\theta)}_{(i,d)}}$) at 3 km intervals from the stations. (*) Correlation is significant at the 0.01 level; (o) Correlation is significant at the 0.05 level.

$\overline{Ufrac^{(ann)}_{(i,d)}}$ and normalised UHI ($\overline{\Delta T_{i-\mathrm{u}}}$), ($i = 1, \ldots, N_{\mathrm{station}}$; $d = 1$: 0–3 km; $d = 2$: 4–6 km; ... $d = 5$: 13–15 km) Figure 7(a). The strongest relation is found at the 0–3 km urban fraction range in all wind speed groups. The strength of the correlation is shown to decline quickly thereafter with distance. For WG1 and WG2 groups the correlation is only significant at the 0.01 level at 0–3 km distance. Correlations significant at the 0.01 level extend to 7–9 km under WG3. These results indicate that the UHI at each site is strongly related to the local land use up to 3 km for WG1 and WG2 and 9 km for WG3. This is in line with our prior understanding that (excluding meteorological factors) UHIs are predominantly controlled by local land use.

To determine the distance from which the additional UHA term may influence temperature at a station, the same correlation analysis is conducted between the Ufrac arcs ($\overline{\Delta Ufrac^{(\theta)}_{(i,d)}}$) and mean UHA ($\overline{T^{(\theta)}_{UHA\ (i)}}$), Figure 7(b). In this analysis, data from all wind sectors (θ) are combined. No correlations significant at the 0.01 level are found closest to the stations (0–3 km) in any wind speed group. This corresponds to how UHA has been defined (see Figure 2) and confirms that the local UHI component has been effectively removed. The correlation strength increases and is significant to the 0.01 level for all wind speed groups at distances 4–6 km from the stations. This indicates the UHA distance at which Ufrac begins to influence UHA. For WG1, correlations are strongest at 4–9 km from the stations, i.e. UHA advection from distant sources will be diminished. For WG2, the highest correlation is at 7–9 km and it remains high until 10–12 km. For WG3, the highest correlation is shifted to 13–15 km, i.e. increased wind speed transports heat further. As such, each wind speed group has its own characteristic UHA distance: the higher the wind speed, the larger the distance. With peak UHA observed in WG2, the UHA distance analysis shows that the downwind UCL warming from the city in this group will be experienced in rural areas up to 12 km away. These distances are calculated based on the mean UHA pattern, therefore on an individual night these distance would be variable. For example modelling the UHI of a significantly larger city, London, has shown UHA can extend as far as 40 km downwind (Bohnenstengel *et al.*, 2011).

4. Conclusions

The complex nature of urban environments provides intrinsic challenges in quantifying UHA. To address this, a new high-density network of urban weather stations (BUCL) in Birmingham has been used to quantify both UHI and UHA at a sub-city scale. The unique spatial and temporal aspects of this dataset has shown Birmingham to exhibit a large mean nocturnal UHI intensity of up to 4.3 °C under low wind speeds and clear skies over 20 consecutive months.

Overall, using the novel methodology outlined, a clear spatial pattern of long-term averaged UHA (the advection-induced UHI component separated from the locally heated UHI component) is found across the city, with a maximum magnitude of 1.18 °C. The peak UHA influence is found under the medium-wind group (WG2), with a mean UHA signal of 0.4 °C, and with 25% of stations experiencing between 0.5 and 1.2 °C. The maximum UHA found in WG2 rather than WG1 (the low-wind group) could be explained by a reduced capacity to advect heat for WG1. For the high-wind group (WG3), however, UHI intensities are vastly reduced due to increased atmospheric mixing, thus leaving little heat for advection. Whilst these observations establish that UHA in the UCL is a significant phenomenon, the processes at which heat is transported (i.e. horizontally through the UCL or mixed downwards from the urban plume) cannot be identified in this study. However the correlation methodology based on urban fraction data is able to show that the total UHI component at a given location is a construct of the urban heat created by local land use and heat advected from upstream sources, with distance dependent on wind speed. With distances over 10 km at which the advection signal is still present, this has considerable implications not only for long-term climate records taken near cities, but for adapting cities and protecting vulnerable citizens in a changing climate.

Although UHA has previously been difficult to quantify and is not always considered in UHI studies due to the lack of urban meteorological observations, this article has successfully demonstrated UHA to be a substantial and noteworthy urban climate process. The unique methodology developed in this article (i.e. use of urban reference temperatures and techniques to isolate UHA only previously used in mesoscale modelling approaches) can be readily adapted to other urban networks worldwide.

Acknowledgements

This research was principally supported by a Natural Environment Research Council CASE (collaborative award in science and engineering) studentship (grant number NE/K008056/1). The research was also part funded by Birmingham City Council, and the National Institute for Health Research Health Protection Research Unit (NIHR HPRU) in Environmental Change and Health at the London School of Hygiene and Tropical Medicine in partnership with Public Health England (PHE), and in collaboration with the University of Exeter, University College London, and the Met Office. The views expressed are those of the author(s) and not necessarily those of the NHS, the NIHR, the Department of Health or Public Health England. We thank Birmingham Urban Climate Laboratory for providing AWS data and the British Atmospheric Data Centre for Met Office station data.

References

Ackerman B, Changnon SA, Dzurisin G Jr, Gatz DF, Grosh RC, Hilberg SD, Huff FA, Mansell JW, Ochs HT III, Peden ME, Schickedanz PT, Semonin RG, Vogel JL. 1978. *Summary of METROMEX. Volume 2: Causes of Precipitation Anomalies*. Bulletin 63. Illinois State Water Survey: Urbana, IL.

Arnfield AJ. 2003. Two decades of urban climate research: A review of turbulence, exchanges of energy and water, and the urban heat island. *Int. J. Climatol.* **23**: 1–26, doi: 10.1002/joc.859.

Azevedo JA, Chapman L, Muller CL. 2016. Quantifying the daytime and nighttime urban heat island in Birmingham, UK: A comparison of satellite derived land surface temperature and high resolution air temperature observations. *Remote Sens.* **8**: 153, doi: 10.3390/rs8020153.

Barlow JF. 2014. Progress in observing and modelling the urban boundary layer. *Urban Clim.* **10**: 216–240, doi: 10.1016/j.uclim.2014.03.011.

Bohnenstengel SI, Evans S, Clark PA, Belcher SE. 2011. Simulations of the London urban heat island. *Q. J. R. Meteorol. Soc.* **137**: 1625–1640, doi: 10.1002/qj.855.

Bornstein RD, Johnson SD. 1977. Urban–rural wind velocity differences. *Atmos. Environ.* **11**: 597–602, doi: 10.1016/0004-6981(77)90112-3.

Brandsma T, Wolters D. 2012. Measurement and statistical modeling of the urban heat island of the city of Utrecht (the Netherlands). *J. Appl. Meteorol. Clim.* **51**: 1046–1060, doi: 10.1175/JAMC-D-11-0206.1.

Brandsma T, Konnen GP, Wessels HRA. 2003. Empirical estimation of the effect of urban heat advection on the temperature series of De Bilt (The Netherlands). *Int. J. Climatol.* **23**: 829–845, doi: 10.1002/joc.902.

Chandler TJ. 1965. *The Climate of London*. Hutchinson: London. doi: 10.1177/0309133309339794.

Chapman L, Azevedo JA, Prieto-Lopez T. 2013. Urban heat and critical infrastructure networks: A viewpoint. *Urban Clim.* **3**: 7–12, doi: 10.1016/j.uclim.2013.04.001.

Chapman L, Muller CL, Young DT, Warren EL, Grimmond CSB, Cai X-M, Ferranti JS. 2014. The Birmingham Urban Climate Laboratory: An open meteorological testbed and challenges of the smart city. *Bull. Am. Meteorol. Soc.* **96**: 1545–1560, doi: 10.1175/BAMS-D-13-00193.1.

Chemel C, Sokhi RS. 2012. Response of London's urban heat island to a marine air intrusion in an easterly wind regime. *Boundary-Layer Meteorol.* **144**: 65–81, doi: 10.1007/s10546-012-9705-x.

Chen XL, Zhao HM, Li PX, Yin ZY. 2006. Remote sensing image-based analysis of the relationship between urban heat island and land use/cover changes. *Remote Sens. Environ.* **104**: 133–146, doi: 10.1016/j.rse.2005.11.016.

Ching JKS, Clarke JF, Godowitch JM. 1983. Modulation of heat flux by different scales of advection in an urban environment. *Boundary-Layer Meteorol.* **25**: 171–191, doi: 10.1007/BF00123973.

Clarke JF. 1969. Nocturnal urban boundary layer over Cincinnati, Ohio. *Mon. Weather Rev.* **97**: 582–589, doi: 10.1175/1520-0493(1969)097<0582:NUBLOC>2.3.CO;2.

Dirks RA. 1974. Urban atmosphere: Warm dry envelope over St. Louis. *J. Geophys. Res.* **79**: 2156–2202, doi: 10.1029/JC079i024p03473.

Garratt JR. 1990. The internal boundary layer – a review. *Boundary-Layer Meteorol.* **50**: 171–203, doi: 10.1007/BF00120524.

Gedzelman SD, Austin S, Cernak R, Stefano N, Partridge S, Quesenberry S, Robinson DA. 2003. Mesoscale aspects of the urban heat island around New York City. *Theor. Appl. Climatol.* **75**: 29–42, doi: 10.1007/s00704-002-0724-2.

Godowitch JM, Ching JKS, Clarke JF. 1987. Spatial variation of the evolution and structure of the urban boundary layer. *Boundary-Layer Meteorol.* **38**: 249–272, doi: 10.1007/BF00122447.

Grimmond CSB, Roth M, Oke TR, Au YC, Best M, Betts R, Carmichael G, Cleugh H, Dabberdt W, Emmanuel R, Freitas E, Fortuniak K, Hanna S, Klein P, Kalkstein LS, Liu CH, Nickson A, Pearlmutter D, Sailor D, Voogt J. 2010. Climate and more sustainable cities: Climate information for improved planning and management of cities (producers/capabilities perspective). *World Clim. Conf.* **3**: 247–274, doi: 10.1016/j.proenv.2010.09.016.

Haeger-Eugensson M, Holmer B. 1999. Advection caused by the urban heat island circulation as a regulating factor on the nocturnal urban heat island. *Int. J. Climatol.* **19**: 975–988, doi: 10.1002/(SICI)1097-0088(199907)19:9<975::AID-JOC399>3.0.CO;2-J.

Hajat S, Vardoulakis S, Heaviside C, Eggen B. 2014. Climate change effects on human health: Projections of temperature-related mortality for the UK during the 2020s, 2050s and 2080s. *J. Epidemiol. Commun. Health* **68**: 641–648, doi: 10.1136/jech-2013-202449.

Heaviside C, Cai X-M, Vardoulakis S. 2015. The effects of horizontal advection on the urban heat island in Birmingham and the West Midlands, United Kingdom during a heatwave. *Q. J. R. Meteorol. Soc.* **141**: 1429–1441, doi: 10.1002/qj.2452.

Heaviside C, Vardoulakis S, Cai X-M. 2016. Attribution of mortality to the Urban Heat Island during heatwaves in the West Midlands, UK. *Environ. Health* **15**: 27, doi: 10.1186/s12940-016-0100-9.

Hidalgo J, Masson V, Gimeno L. 2010. Scaling the daytime urban heat island and urban-breeze circulation. *J. Appl. Meteorol.* **49**: 889–901, doi: 10.1175/2009JAMC2195.1.

Hildebrand PH, Ackerman B. 1984. Urban effects on the convective boundary layer. *J. Atmos. Sci.* **41**: 76–91, doi: 10.1175/1520-0469(1984)041<0076:UEOTCB>2.0.CO;2.

Johnson H, Kovats RS, McGregor G, Stedman J, Gibbs M, Walton H, Cook L, Black E. 2005. The impact of the 2003 heat wave on mortality and hospital admissions in England. *Health Stat. Q.* **25**: 6–11.

Kalnay E, Cai M. 2003. Impact of urbanization and land-use change on climate. *Nature* **423**: 528–531, doi: 10.1016/j.uclim.2013.04.00.1.

Knight S, Smith C, Roberts M. 2010. Mapping Manchester's urban heat island. *Weather* **65**: 188–193, doi: 10.1002/wea.542.

Lowry WP. 1977. Empirical estimation of urban effects on climate: A problem analysis. *J. Appl. Meteorol.* **16**: 129–135, doi: 10.1175/1520-0450(1977)016<0129:EEOUEO>2.0.CO;2.

Muller CL, Chapman L, Grimmond CSB, Young DT, Cai X-M. 2013. Toward a standardized metadata protocol for urban meteorological networks. *Bull. Am. Meteorol. Soc.* **94**: 1161–1185, doi: 10.1175/BAMS-D-12-00096.1.

Oke TR. 1973. City size and the urban heat island. *Atmos. Environ.* **7**: 769–779, doi: 10.1016/0004-6981(73)90140-6.

Oke TR. 1976. The distinction between canopy and boundary-layer urban heat islands. *Atmosphere* **14**: 268–277, doi: 10.1080/00046973.1976.9648422.

Oke TR. 1982. The energetic basis of the urban heat island. *Q. J. R. Meteorol. Soc.* **108**: 1–24, doi: 10.1002/qj.49710845502.

Oke TR. 2006. 'Initial guidance to obtain representative meteorological observations at urban sites.' IOM Report No. 81, WMO/TD. No. 1250. World Meteorological Organization: Geneva.

ONS (Office for National Statistics). 2013. '2011 Census analysis – comparing rural and urban areas of England and Wales.' http://www.ons.gov.uk/ons/dcp171776_337939.pdf (accessed 3 November 2015).

Pasquill F, Smith FB. 1983. *Atmospheric Diffusion* (3rd edn). Ellis Horwood Limited: Chichester, UK, doi: 10.1002/qj.49711046416.

Robine J-M, Cheung SL, Le Roy S, Van Oyen H, Griffiths C, Michel JP, Herrmann FR. 2008. Death toll exceeded 70,000 in Europe during the summer of 2003. *C.R. Biol.* **331**: 171–175, doi: 10.1016/j.crvi.2007.12.001.

Stewart ID. 2011. A systematic review and scientific critique of methodology in modern urban heat island literature. *Int. J. Climatol.* **31**: 200–217, doi: 10.1002/joc.2141.

Stewart ID, Oke TR. 2012. Local climate zones for urban temperature studies. *Bull. Am. Meteorol. Soc.* **93**: 1879–1900, doi: 10.1175/BAMS-D-11-00019.1.

Szymanowski M, Kryza M. 2009. GIS-based techniques for urban heat island spatialization. *Clim. Res.* **38**: 171–187, doi: 10.3354/cr00780.

Takane Y, Ohashi Y, Kusaka H, Shigeta Y, Kikegawa Y. 2013. Effects of synoptic-scale wind under the typical summer pressure pattern on the mesoscale high-temperature events in the Osaka and Kyoto urban areas by the WRF Model. *J. Appl. Meteorol. Clim.* **52**: 1764–1778, doi: 10.1175/JAMC-D-12-0116.1.

Thornes T. 2015. Variations of temperature, wind speed and humidity within Birmingham New Street Station during hot weather. *Weather* **70**: 129–134, doi: 10.1002/wea.2358.

Tomlinson CJ, Chapman L, Thornes JE, Baker CJ. 2012. Derivation of Birmingham's summer surface urban heat island from MODIS satellite images. *Int. J. Climatol.* **32**: 214–224, doi: 10.1002/joc.2261.

Tomlinson CJ, Prieto-Lopez T, Bassett R, Chapman L, Cai X-M, Thornes JE, Baker CJ. 2013. Showcasing urban heat island work in Birmingham – measuring, monitoring, modelling and more. *Weather* **68**: 44–49, doi: 10.1002/wea.1998.

Unger J, Sumeghy Z, Szegedi S, Kiss A, Geczi R. 2010. Comparison and generalisation of spatial patterns of the urban heat island based on normalized values. *Phys. Chem. Earth* **35**: 107–114, doi: 10.1016/j.pce.2010.03.001.

Vaisala. 2012. 'Vaisala weather transmitter WXT520 user's guide.' http://www.vaisala.com/Vaisala%20Documents/User%20Guides%20and%20Quick%20Ref%20Guides/M210906EN-C.pdf (accessed 21 February 2016).

Warren EL, Chapman L, Young DT, Muller CL, Cai X-M, Grimmond CSB. 2016. The Birmingham Urban Climate Laboratory – a high density, urban meteorological dataset, from 2012–2014. *Nat. Sci. Data* 3: 160038, doi: 10.1038/sdata.2016.38.

Wong KK, Dirks RA. 1978. Mesoscale perturbations on airflow in the urban mixing layer. *Bull. Am. Meteorol. Soc.* **17**: 677–688, doi: 10.1175/1520-0450(1978)017<0677:MPOAIT>2.0.CO;2.

Zhang D-L, Shou Y-X, Dickerson RR. 2009. Upstream urbanization exacerbates urban heat island effects. *Geophys. Res. Lett.* **36**: L24401, doi: 10.1029/2009GL041082.

Zhou LM, Dickinson RE, Tian Y, Fang J, Li Q, Kaufmann RK, Tucker CJ, Myneni RB. 2004. Evidence for a significant urbanization effect on climate in China. *Proc. Natl. Acad. Sci. U.S.A.* **101**: 9540–9544, doi: 10.1073/pnas.0400357101.